Heterogeneous Reaction of Gaseous Nitric Acid on γ-Phase Iron(III) Oxide

Elizabeth K. Frinak, Sandra J. Wermeille, Courtney D. Mashburn, and Margaret A. Tolbert*

CIRES and Department of Chemistry and Biochemistry, University of Colorado, Boulder, Colorado 80309

Christopher J. Pursell

Department of Chemistry, Trinity University, San Antonio, Texas 78212

Received: June 30, 2003; In Final Form: October 1, 2003

The uptake of HNO_3 on γ-Fe_2O_3 particles that model atmospheric mineral dust has been investigated using FT-IR spectroscopy and mass spectrometry to probe the condensed and gas phases, respectively. To accurately calculate the HNO_3 saturation coverage (θ) and initial uptake coefficient (γ), the specific surface area of γ-Fe_2O_3 was measured in situ using water as an adsorbate. The saturation coverage of HNO_3 on γ-Fe_2O_3 was found to be $\theta = (1.1 \pm 0.9) \times 10^{14}$ molecules/cm^2 and the initial uptake coefficient was found to be $\gamma = (1.5 \pm 1.0) \times 10^{-5}$ at 297 K and $P_{HNO_3} = 1 \times 10^{-5}$ Torr. These values were slightly larger at 220 K for the same partial pressure of nitric acid. Spectroscopically, HNO_3 was observed to bind to the surface in the form of nitrate ions. The significance of this reaction to tropospheric chemistry is discussed.

I. Introduction

Windblown sediments in semi-arid and arid regions contribute an estimated 2000 Tg/yr of mineral aerosol to the atmosphere.[1,2] The particles range in radius from 0.005 to 20 μm.[3] Particles exceeding a radius of 10 μm are redeposited within the source region, leaving approximately 350 Tg/yr available for long-range transport on a time scale of days to weeks.[4]

Once in the free troposphere, mineral aerosol particles are of interest for several reasons. First, they may impact the climate either directly or indirectly. Direct effects result from the absorption or scattering of solar or terrestrial radiation.[5] Indirectly, mineral aerosol may modify cloud properties, which in turn could affect climate.[6,7] Recent studies have also shown that mineral aerosol may affect ice nucleation processes.[8] In addition to the possible effects on climate, minerals may also impact the chemistry of the troposphere. Nitrogen oxides have been the focus of some heterogeneous chemistry studies because of discrepancies in measured and modeled values and the influence of these values on tropospheric ozone levels.

NO and NO_2 are short-lived species that rapidly interchange and are collectively termed NO_x.[9] Because NO_2 leads to the formation of tropospheric O_3, a full understanding of the NO_x budget is needed to predict tropospheric O_3 levels. At present, models overestimate the ratio of HNO_3 to NO_x by a factor of 5−10, with the overestimation being much larger in the summer than in the winter.[10,11] One possible reason for the discrepancy between measured and modeled ratios of HNO_3 and NO_x is an unidentified heterogeneous loss or missing sink of HNO_3. Reactions on mineral aerosol have been proposed as an explanation of why there is an increased overestimation of the ratio in the summer when dust loadings are higher.[1]

Maghemite (γ-Fe_2O_3), one of the four polymorphs of iron(III) oxide, was used as the model mineral surface in these studies. It is the ferrimagnetic cubic form of iron(III) oxide[12] and is commonly found in Chinese loess deposits.[13,14] It is also a product of slash-and-burn fires when goethite is a constituent of the topsoil and is burned in the presence of organic matter.[15]

Previous studies have investigated the adsorption of HNO_3 to α-Fe_2O_3 and γ-Fe_2O_3 surfaces among other metal oxides. Underwood et al. have reported an initial uptake coefficient for HNO_3 on α-Fe_2O_3 of $\gamma = 5.3 \times 10^{-5}$ and saturation coverage of $\theta = 6.9 \times 10^{13}$ molecules/cm^2 at a nitric acid pressure of 1×10^{-5} Torr.[16] A slightly larger saturation coverage value of $\theta = 3 \times 10^{14}$ molecules/cm^2 was measured by Goodman et al. for HNO_3 on γ-Fe_2O_3.[17] Studies on metal oxides and mineral dust have also been performed by Hanisch and Crowley.[18,19] For comparison, Hanisch and Crowley report a $\gamma = 0.13$ for the uptake of HNO_3 on α-Al_2O_3.[18] However, Underwood et al. report $\gamma = 9.1 \times 10^{-6}$ for the same reaction on the same substrate.[20] A possible reason for this major discrepancy is the different surface area assumed by the two groups. Underwood et al.[20] and Goodman et al.[17] find a mass-dependent uptake and use the BET surface area to determine θ and γ. In contrast, Hanisch and Crowley find a mass-independent uptake and use the geometric surface area of the sample in their calculations.[18,19] It is therefore unresolved in the literature whether the entire BET surface area is available for these reactions.

Our study differs from the previous work in that we first measured the specific surface area of the γ-Fe_2O_3 powder samples in situ using a water vapor adsorption method. This measurement was significant for two main reasons. This eliminated the need to assume a surface area for the samples. In addition, by performing the measurement in situ, any changes in the surface area due to sample preparation were taken into account. The water uptake was probed simultaneously using both mass spectrometry and Fourier transform infrared spectroscopy. Following determination of the specific surface area, the reaction between HNO_3 and γ-Fe_2O_3 was characterized as a function of sample mass, temperature, and partial pressure of HNO_3.

II. Experimental Section

A. Vacuum Chamber. Experiments were performed in a high-vacuum chamber with Knudsen cell capabilities shown schematically in Figure 1. A combination of Fourier transform

* To whom correspondence should be addressed.

10.1021/jp030807o CCC: $27.50
Published on Web 02/10/2004

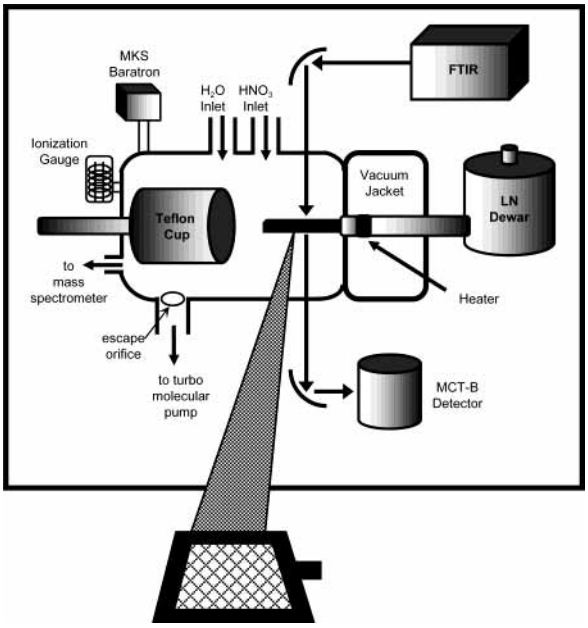

Figure 1. Schematic diagram of the Knudsen cell reactor.

infrared (FT-IR) spectroscopy and mass spectrometry was used to probe the condensed and gas phases, respectively. The main chamber houses a UTI 100C electron impact ionization quadrupole mass spectrometer to monitor the partial pressures of gas-phase species as well as an ionization gauge and an MKS Baratron for the measurement of total chamber pressure. The chamber is pumped through an escape orifice of effective area $A_h = 0.16$ cm^2 using a 150 L/s turbomolecular pump (Pfeiffer). The γ-Fe_2O_3 sample was supported on a tungsten mesh that was sandwiched between two copper plates held tightly together by stainless steel clips. Indium foil was placed between the tungsten mesh and the mount to improve thermal contact. The entire assembly was attached to a liquid nitrogen cooled cryostat. Heating against the liquid nitrogen occurred on the backside of the sample support inside the vacuum jacket. This ensured that the entire sample and mount assembly in the main chamber was at a uniform temperature. Two type-T thermocouples were attached to the copper support to monitor the temperature. Temperature could be controlled between 100 K and room temperature using a Eurotherm temperature controller. The γ-Fe_2O_3 sample can be isolated from the gas flow by covering it with a Teflon cup. With use of an O-ring, the Teflon cup seals against the stainless steal vacuum jacket, allowing a constant signal of H_2O or HNO_3 to be established without exposing the sample to the reactant gas.

B. Sample Preparation. The γ-Fe_2O_3 sample was prepared by either pressing or depositing γ-Fe_2O_3 (Nanophase Technologies, 99.5%, diameter of 26 nm) onto a 2 cm $\times$ 2 cm tungsten mesh. Three different sizes of tungsten wire mesh were used to vary the mass of the pressed samples. The sizes used were 150 mesh ($d = 0.0008$ in.), 80 mesh ($d = 0.0015$ in.), and 40 mesh ($d = 0.003$ in.). All three had a throughput of 77% and were provided by UNIQUE Wire Weaving. The 80 mesh was used for all of the deposited samples. Deposited samples were made by preparing slurries of either water or methanol and γ-Fe_2O_3 into which the mesh was dipped. Figure 2 shows scanning electron microscope (SEM) images of a blank mesh and a sample prepared by depositing γ-Fe_2O_3 onto the mesh from a methanol slurry. The images show the irregular morphology of the reactive γ-Fe_2O_3 surface. Though not shown, images were also collected using transmission electron microscopy (TEM). The TEM images confirmed the γ-Fe_2O_3 particle diameter of

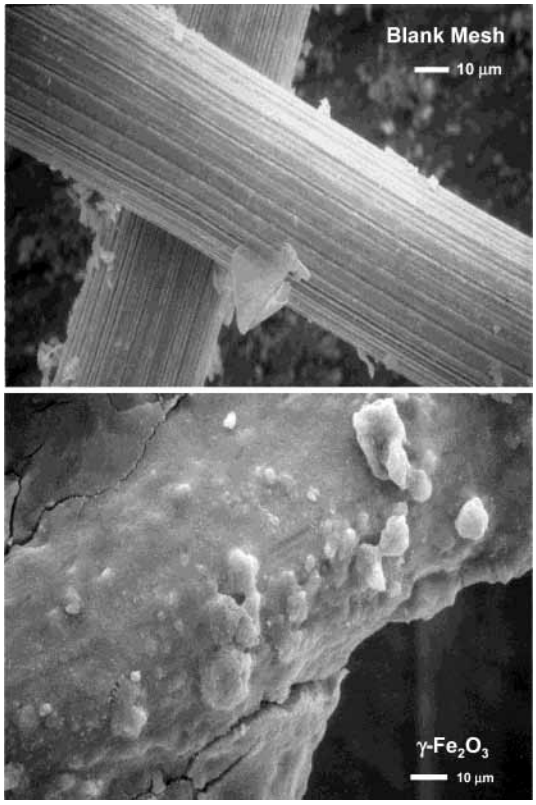

Figure 2. SEM images of blank mesh and mesh coated with γ-Fe_2O_3. Both use a mesh with a wire diameter of 0.0015 in. and 80 openings per inch.

26 nm reported by the manufacturer. Samples were dried at room temperature until placed in the vacuum chamber and dried overnight at a total pressure of 5×10^{-7} Torr.

C. Mass Spectrometer Data. A typical experiment began with passivation of the chamber walls. During passivation, the Teflon cup was closed, isolating the sample from the gas flow, and the reactive gas of interest was leaked into the chamber for 90 min until the flow was stable, as observed in the mass spectrometer signal. After a constant flow was established, the Teflon cup was retracted, exposing the sample to the gas flow for a period of 30 min. The cup was then closed to re-establish a baseline signal and the procedure was repeated several times. Some samples were exposed for longer periods of time, up to 3 h, to determine the best fitting method to analyze the data.

Coverage (θ) on γ-Fe_2O_3 was determined by integrating the mass spectrometer signal when the Teflon cup was open to determine the loss of reactant from the gas phase. Coverages were corrected for loss to the sample mount by subtracting values from blank experiments. Blank experiments consisted of uptake onto a tungsten mesh that contained no γ-Fe_2O_3.

Initial uptake coefficients (γ) were calculated from the data using the mass spectrometer signal before (I_o) and during (I) uptake. The values presented in this paper represent the uptake coefficient as calculated upon initial exposure of the sample. At low sample masses, the uptake coefficient was found to vary linearly with mass. After correction for the blank experiments, a plot of $(I_o - I)/I$ as a function of sample mass was generated. The slope of this line was used to calculate the uptake coefficient using eq 1.[20]

$$\gamma = \left(\frac{A_h}{\text{SSA} \times \text{mass}}\right)\left(\frac{I_o - I}{I}\right) \quad (1)$$

In eq 1, SSA refers to the specific surface area (cm^2/mg) and

A_h is the effective area of the escape orifice. As previously mentioned, it is important to use the appropriate value for the surface area. The geometric surface area of the tungsten mesh used in these experiments was approximately 4 cm^2 based on the mesh wire dimensions. However, the BET surface area of γ-Fe_2O_3 is 450 cm^2/mg. This value was reported by the manufacturer for the bulk powder and independently confirmed by the authors using a volumetric expansion technique with N_2 as the adsorbate. With use of the BET surface area value, a 10-mg sample of bulk powder has a surface area of 4500 cm^2. Values for θ and γ can therefore vary by as much as 3 orders of magnitude depending on whether the geometric surface area or a surface area calculated from the BET surface area is used in the calculation. To report accurate values for θ and γ, the specific surface area of samples of γ-Fe_2O_3 was measured in situ using water as an adsorbate.

D. FT-IR Measurements. While the Teflon cup was open, the condensed phase products were monitored by transmission FT-IR spectroscopy. Spectra were acquired using a single-beam Nicolet 740 spectrometer equipped with an MCT-B detector. For all experiments, 32 scans were collected at a resolution of 4 cm^{-1} from 4000 to 400 cm^{-1}. Formation of products was observed by taking the ratio of a single-beam sample background of the γ-Fe_2O_3 collected prior to exposure to scans collected during exposure. For the specific surface area measurement, the peak area of the O−H stretching vibrational mode was integrated over time over the wavenumber range 2400−3630 cm^{-1} to determine coverage. For the HNO_3 uptake study, the wavenumber range 1100−1400 cm^{-1} was used.

III. Results and Discussion

A. In Situ Specific Surface Area Measurement. On the basis of a study of soil specific surface area by Newman, water was used as the adsorbate to measure the specific surface area of γ-Fe_2O_3.[21] With knowledge of the size of a water molecule, the mass of the sample, and total amount of water adsorbed for monolayer coverage, the specific surface area can be determined.[17,21] Specific surface area measurements were performed on γ-Fe_2O_3 samples ranging in mass from 5 to 92 mg. For these experiments, the chamber was first passivated for 60 min with water (Fisher Scientific, HPLC grade). The passivation was considered complete when the water signal was stable as observed in the mass spectrometer at $m/e = 18$. Following passivation, samples were exposed in 30-min cycles until equilibrium was reached, as indicated by the mass spectrometer and FT-IR signals.

To work at pressures appropriate for the mass spectrometer, experiments were performed at 200 K. On the basis of literature work at room temperature, a monolayer was expected to form on the γ-Fe_2O_3 surface at 13% relative humidity with respect to water.[17,21] At 200 K, 13% relative humidity corresponds to a water pressure of 3.2×10^{-4} Torr. At this temperature, the saturation vapor pressure of ice is 1.2 mTorr. Our experiments were performed at water pressure lower than this, preventing multilayer formation. To account for possible temperature dependence in the monolayer coverage, a pressure study was performed to determine the pressure at which one monolayer of water is adsorbed to the γ-Fe_2O_3 surface at 200 K. Figure 3 shows representative mass spectrometer data for exposure of a 13.4-mg γ-Fe_2O_3 sample and a blank to water at 200 K and a pressure of approximately 1×10^{-4} Torr. It can be seen that much more water adsorption occurred on the sample than on the blank so that only a very small blank correction was necessary. Experiments were performed over a range of water

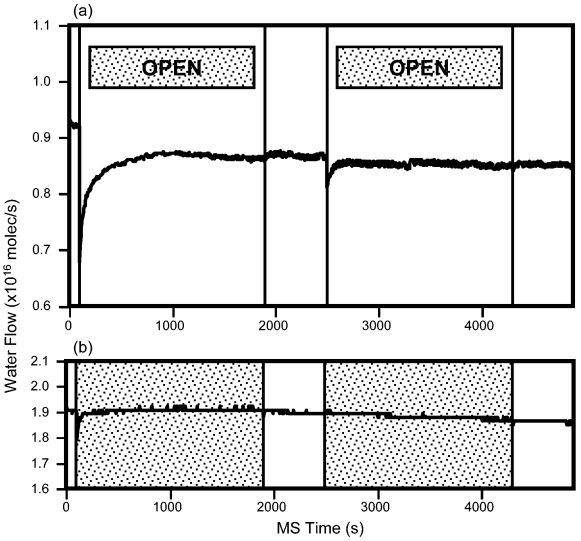

Figure 3. Typical signals for H_2O uptake (a) on a methanol-deposited γ-Fe_2O_3 sample ($P_{H_2O} = 1.12 \times 10^{-4}$ Torr, $m_{Fe_2O_3} = 13.4$ mg, $T = 200$ K) and (b) on a blank mesh ($P_{H_2O} = 2.5 \times 10^{-4}$ Torr, $T = 200$ K).

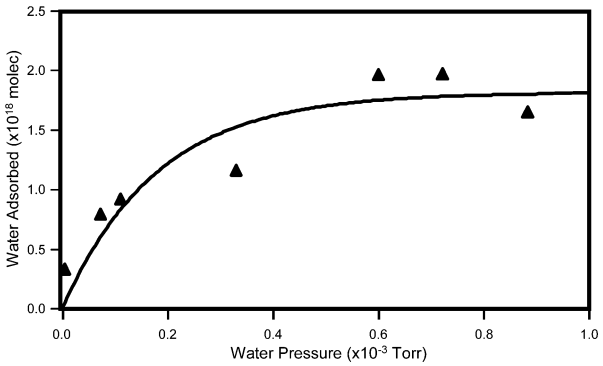

Figure 4. Water uptake on 13.4 mg of γ-Fe_2O_3 as a function of water pressure at 200 K. Sample was prepared by depositing γ-Fe_2O_3 from a methanol slurry.

TABLE 1: Measured Values for Specific Surface Area of γ-Fe_2O_3 from the Mass Spectrometer Data

mass γ-Fe_2O_3 (mg)	H_2O adsorbed ($\times 10^{18}$ molecule)	surface area (cm^2)	specific surface area (cm^2/mg)
5.1[a]	1.42	1507	295
9.55[a]	3.01	3195	335
13.4[a]	1.97	2079	156
92.0[b]	8.35	8850	96

[a] Samples prepared by depositing γ-Fe_2O_3 on mesh from methanol slurry. [b] Sample prepared by pressing γ-Fe_2O_3 on mesh.

pressure and integrations of the total adsorbed water for each exposure are shown in Figure 4. This study shows that one monolayer of water corresponds to 1.97×10^{18} water molecules adsorbed to the 13.4-mg sample as determined from the fit to the data. The curve in Figure 4 was not extended to multilayer coverage due to the experimental limitation of the mass spectrometer and to avoid the condensation of ice. Assuming one molecule of water is a sphere with a surface area of 1.06×10^{-15} cm^2/molecule,[21] the 13.4-mg sample has a specific surface area of 156 cm^2/mg for this sample.

With use of the mass spectrometer, the specific surface was measured over a range of sample masses and the results are summarized in Table 1. Notice the two lowest mass samples have very similar specific surface areas, but these values decrease for the high mass samples. This indicates that the entire sample surface area is not accessible for adsorption at masses

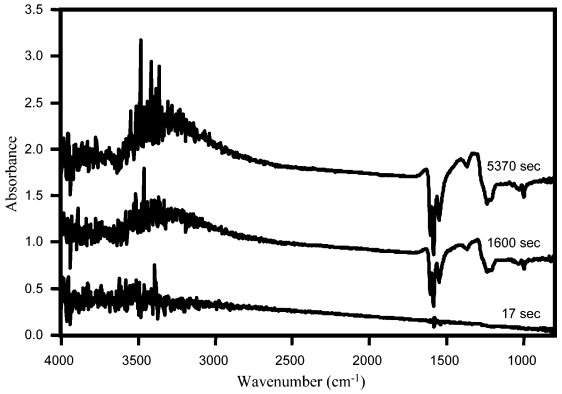

Figure 5. Growth of adsorbed water peaks with time in the infrared spectra during exposure of γ-Fe_2O_3 to water ($m_{Fe_2O_3} = 92.0$ mg, $T =$ 200 K, $P_{H_2O} = 6.7 \times 10^{-4}$ Torr). Scales are offset for clarity.

greater than 10 mg. Also notice the variability in the surface area as the sample masses transition from the linear mass-dependent region into the mass independent region. This is potentially due to sample preparation as variations may have occurred in ambient temperature and humidity during preparation. However, we are interested in the specific surface area in the linear mass-dependent region, where the entire surface is available for reaction, so the variations outside of this region are of little concern. The specific surface area used for this study is 315 cm^2/mg, which is the average of the first two specific surface area values reported in Table 1. This value is only slightly smaller than the manufacturer's reported BET surface area of 450 cm^2/mg. Therefore, this study shows that, in the absence of in situ specific surface area measurements, the BET surface area provides a close approximation.

The FT-IR data were used to confirm that water lost from the gas phase was adsorbed to the surface and to provide an independent measurement of the specific surface area. Figure 5 shows the FT-IR data collected during exposure of a 92-mg sample of γ-Fe_2O_3 to 6.7×10^{-4} Torr of water at 200 K. The peak extending from 3640 to 2400 cm^{-1} is attributed to the O−H stretching vibrational mode from the adsorbed water. The series of peaks and valleys between 1700 and 900 cm^{-1} are from a combination of H−O−H bending modes and a decrease in the intensity of the γ-Fe_2O_3 absorbance, both of which are the result of surface-adsorbed water. From Beer's Law, we can relate the transmittance to the concentration of water adsorbed,

$$\left(\frac{I}{I_o}\right) = e^{-\alpha x} \qquad (2)$$

where x is the molecules of water per cm^2 probed by the IR beam and α is the base e absorption cross section. To estimate the amount of adsorbed water, we used an absorption cross section of $\alpha = 3.41 \times 10^{-19}$ cm^2/molecule for liquid water at 3350 cm^{-1} and 300 K.[22] We find a water absorbance of $A = \log(I_o/I) = 0.466$ AU at 3350 cm^{-1}, resulting in a surface coverage of water of 3.15×10^{18} molecules/cm^2 over the entire sample. Taking into account the monolayer coverage of 9×10^{14} water molecules/cm^2 [21] and the 92-mg sample mass, we then deduce a specific surface area of 145 cm^2/mg for this sample from the FT-IR data. For this particular experiment, the surface area from the integrated mass spectrometer signal was 96 cm^2/mg. The fairly close proximity of these values confirms that water lost from the gas phase was adsorbed to the γ-Fe_2O_3 surface. This 40% error in specific surface area was used to estimate our error in the determined θ and γ for the HNO_3 uptake experiments.

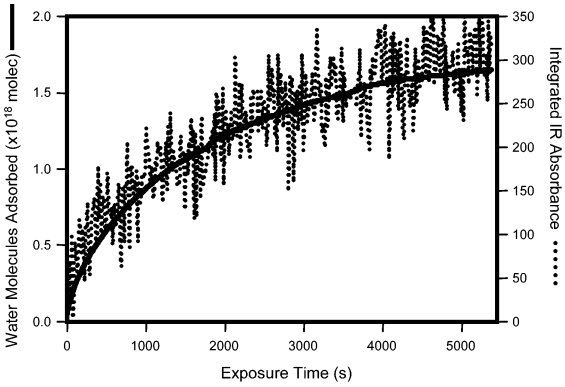

Figure 6. Comparison of MS and IR signals integrated over time. The left axis, which corresponds to the solid line, is the molecules of water adsorbed to the surface as measured in the mass spectrometer at $m/e = 18$. The right axis, which corresponds to the dotted line, is the integrated peak area from 2400 to 3630 cm^{-1}. This peak results from the O−H stretching band. The experimental parameters are described in Figure 5.

Figure 6 shows a direct comparison of the mass spectrometer and FT-IR signals for this experiment. The mass spectrometer signal is represented by the solid line as the cumulative number of water molecules lost from the gas phase during exposure of the sample. The FT-IR signal, depicted by the dotted line, is the integrated peak area for the range from 2400 to 3630 cm^{-1}. This wavenumber region was selected due to the absence of interfering absorbance by the γ-Fe_2O_3. The excellent agreement in the time dependence of these two distinct measurements gives us additional confidence in our specific surface area determination.

B. HNO_3 Uptake Experiments. As with the surface area measurement, a typical HNO_3 experiment begins with passivation of the chamber walls. During passivation, the Teflon cup is closed, isolating the sample from the HNO_3 flow. Nitric acid is leaked into the chamber for 90 min until the HNO_3 flow is stable, as observed in the mass spectrometer signal at a mass-to-charge ratio of $m/e = 46$. After a constant flow is established, the Teflon cup is retracted, exposing the sample to the HNO_3. Samples were exposed in three, 10-min cycles followed by 30-min cycles. Total exposure times ranged from 30 min to 2 h.

HNO_3 uptake experiments were performed as a function of γ-Fe_2O_3 mass, HNO_3 pressure, and substrate temperature. A typical uptake experiment is shown in Figure 7. Figure 7a shows the HNO_3 signal as observed in the mass spectrometer. In this particular experiment, 26.8 mg of γ-Fe_2O_3 was exposed to 1×10^{-5} Torr of HNO_3 at 297 K. Figure 7b shows similar data for a blank experiment which consists of exposure of a tungsten mesh containing no γ-Fe_2O_3 to HNO_3 at a pressure of 1×10^{-5} Torr.

The total coverage was determined by offsetting and inverting the mass spectrometer signal so that the area under the curve represents the amount of HNO_3 adsorbed to the γ-Fe_2O_3 surface.[16] Because of time constraints, the larger mass samples were not exposed to saturation. Saturation was indicated by a complete recovery to baseline in the mass spectrometer signal while the cup was open. An exposure time of 30 min was initially arbitrarily selected. Later, it was realized that 30 min of exposure was not long enough to obtain the double-exponential shape necessary to accurately fit the data.[23] Figure 8 shows the comparison of half an hour of exposure to 2 h and 30 min of exposure for the same experiment. If only 30 min of data is analyzed, a single-exponential fit appears sufficient as shown in Figure 8a. However, after additional exposure time,

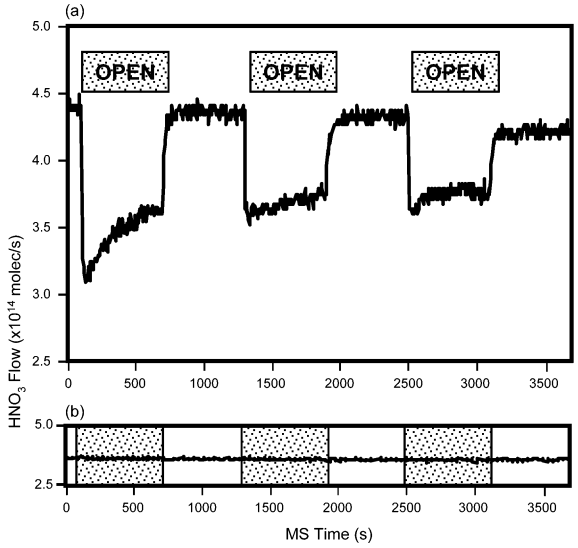

Figure 7. Typical signals for HNO_3 uptake (a) on a γ-Fe_2O_3-coated mesh ($P_{HNO_3} = 1 \times 10^{-5}$ Torr, $m_{Fe_2O_3} = 26.8$ mg, $T = 297$ K) and (b) on a blank mesh ($P_{HNO_3} = 1 \times 10^{-5}$ Torr, $T = 297$ K).

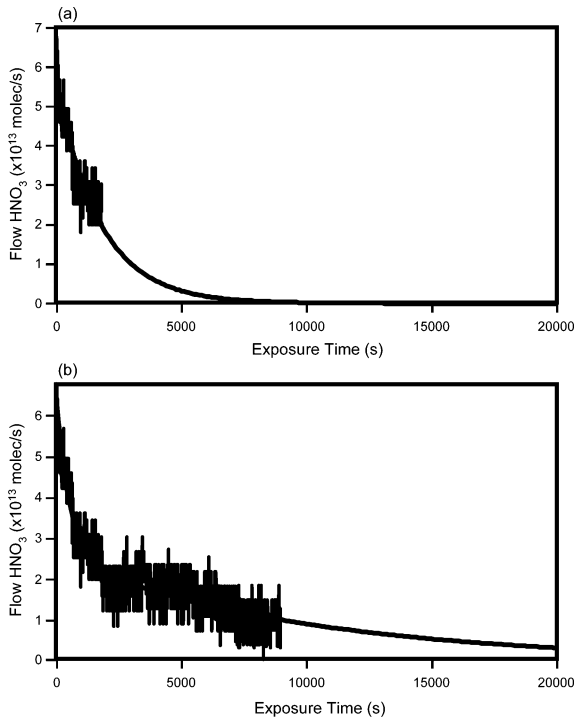

Figure 8. HNO_3 flow as a function of exposure time comparing (a) single- and (b) double-exponential fits. The area under the curve corresponds to coverage. ($P_{HNO_3} = 2 \times 10^{-5}$ Torr, $m_{Fe_2O_3} = 11.4$ mg, $T = 297$ K.)

it becomes apparent that the double-exponential fit is the correct form of the data as shown in Figure 8b. On the basis of a series of long experiments, a correction method was established and applied to the data. The results presented in this paper represent the coverage of the sample as predicted at saturation.

i. Mass Study. The mass study of HNO_3 uptake on γ-Fe_2O_3 was performed in the Knudsen cell reactor at room temperature and a nitric acid pressure of approximately 1×10^{-5} Torr. The mass of γ-Fe_2O_3 ranged from 2 to 150 mg and the results are shown in Figure 9. The different symbols correspond to the different sample preparation methods. As expected from previous studies, the amount of HNO_3 adsorbed was found to increase linearly at low masses.[16,17,20] Samples below 10 mg were considered to be part of this linear mass-dependent regime.

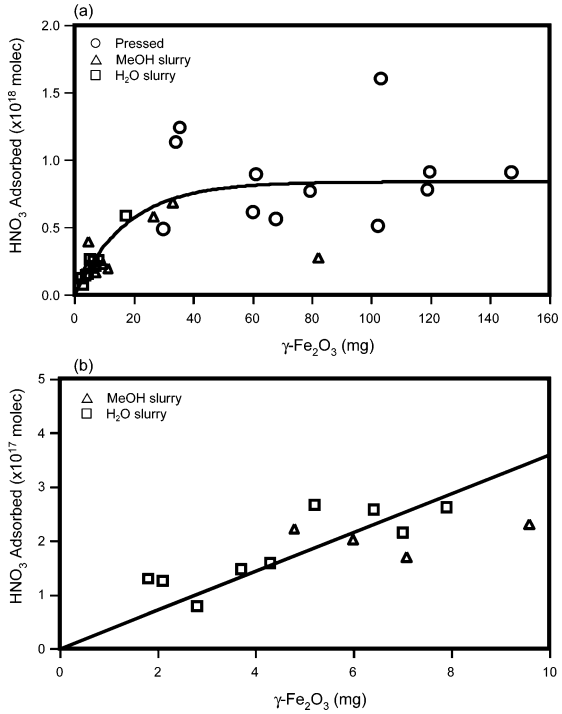

Figure 9. Saturation coverage as a function of γ-Fe_2O_3 mass at 297 K (a) over the entire mass range studied and (b) in the linear mass regime. The different shapes denote the different methods of preparation. ($P_{HNO_3} \sim 1 \times 10^{-5}$ Torr).

Beyond this mass was a plateau region of 8.4×10^{17} molecules adsorbed. Increasing sample mass further had negligible effect on the amount of HNO_3 adsorbed because the entire surface is not available for reaction.

This maximum value is attributed to the inability of the HNO_3 to penetrate throughout all the layers of the sample, resulting in constant coverage despite increasing sample mass. However, at the lower masses, the entire mass of the sample is available for reaction, which leads to the linear correlation between coverage and mass. This behavior was confirmed by the surface area measurement, which showed the apparent decrease in the specific surface area with increasing mass above 10 mg. As mentioned previously, the surface area of the γ-Fe_2O_3 has some variability, especially at masses greater than 10 mg. This variability may account for the scatter in the data in the plateau region. An expanded view of the low mass region is shown in Figure 9b. With use of a line fit through the origin and a specific surface area of 315 cm^2/mg, the saturation coverage was calculated to be 1.1×10^{14} molecules/cm^2 at 297 K. Within error, this value is in excellent agreement with published results for the uptake of HNO_3 on γ-Fe_2O_3.[17]

The initial uptake coefficient was also analyzed as a function of mass at room temperature as shown in Figure 10. With use of the slope from the mass-dependent region, the $(I_o - I)/I$ value may be converted into a γ using eq 1. The initial uptake coefficient for HNO_3 on γ-Fe_2O_3 was calculated to be 1.5×10^{-5} at 297 K. There is currently no value available in the literature for comparison. However, this value is slightly smaller than the value of $\gamma = 5.3 \times 10^{-5}$ reported by Underwood et al. for the uptake of HNO_3 on α-Fe_2O_3.[16]

ii. Temperature Study. The uptake of HNO_3 on γ-Fe_2O_3 was studied over a range of temperatures from 220 to 297 K while maintaining a constant pressure of HNO_3 of 1×10^{-5} Torr. Most of the samples were high mass, pressed samples, but a wider range of masses were studied at 220 K. The results for the saturation coverage, shown in Figure 11a, suggest only a

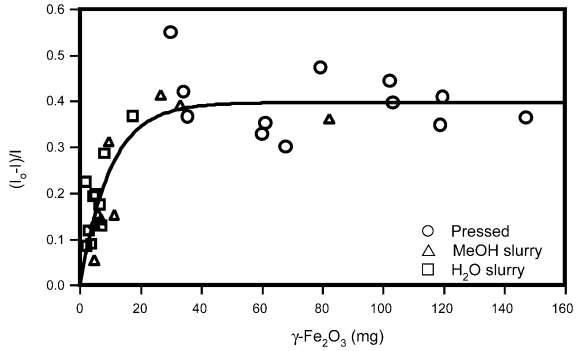

Figure 10. $(I_o - I)/I$ as a function of γ-Fe_2O_3 mass at room temperature over the entire mass range studied. The different shapes denote the different methods of preparation. ($P_{HNO_3} \sim 1 \times 10^{-5}$ Torr).

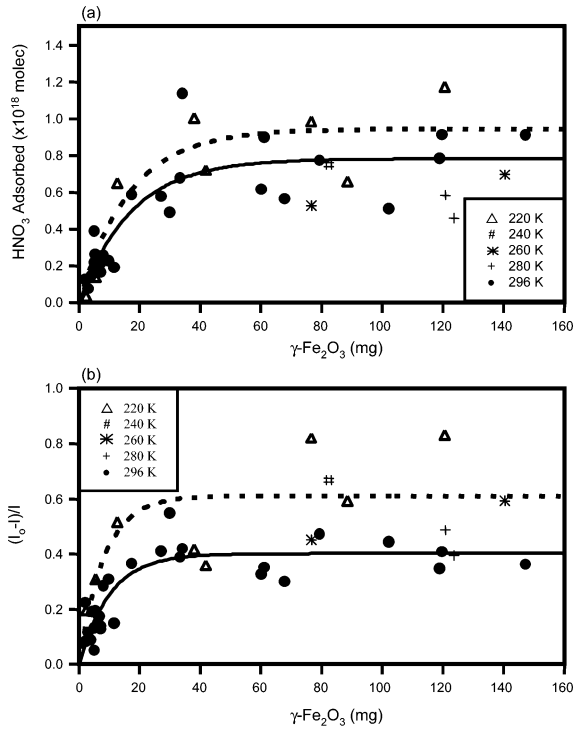

Figure 11. Results from the temperature study for (a) saturation coverage and (b) $(I_o - I)/I$. The dashed line denotes the fit to the data collected at 220 K and the solid line is for data collected at 297 K. ($P_{HNO_3} \sim 1 \times 10^{-5}$ Torr.)

very slight increase in coverage at low temperature with a value of $\theta = 1.4 \times 10^{14}$ molecules/cm^2 at 220 K. The initial uptake coefficient, shown in Figure 11b, also has a mild temperature dependence, increasing with decreasing temperature to a value of $\gamma = 2.9 \times 10^{-5}$ at 220 K. Variability in the sample surface area at higher masses may have affected the plateau regions for both θ and γ.

iii. Pressure Study. A series of experiments at 297 K on pressed samples of approximately 90 mg of γ-FeO_3 were performed under a range of HNO_3 pressures, from 8×10^{-7} to 8×10^{-5} Torr, and the results are summarized in Figure 12. It can be seen in Figure 12 that, within error, the saturation coverage is independent of pressure. It should be noted, however, that the time to reach saturation coverage increases as the pressure decreases. From the results shown in Figure 12, we find the maximum saturated coverage (θ_{max}) of HNO_3 on a γ-Fe_2O_3 surface at room temperature is 8.7×10^{13} molecules/cm^2. This value is in agreement with the coverage of $(1.1 \pm 0.9) \times 10^{14}$ molecules/cm^2 determined in the mass study.

iv. FT-IR Results. In addition to monitoring the gas phase, condensed phase products were monitored when the cup was open using FT-IR spectroscopy. A spectrum of γ-Fe_2O_3 on the tungsten mesh was used as a background. The growth of product peaks was observed by taking the ratio of spectra collected during exposure to HNO_3 to the background. A sample series of spectra from an experiment are shown in Figure 13. The peaks at 1616 and 1282 cm^{-1} are attributed to adsorbed NO_3^-. On the basis of previous publications, these peaks result from the degenerate ν_3 mode of oxide-coordinated nitrate.[17] The nitrate ion has D_{3h} symmetry and may be described as being a plane XY_3 molecule.[24] Upon adsorption to the γ-Fe_2O_3 surface, there is a loss of symmetry, causing a splitting of the peak in the FT-IR spectrum.[11,17] The adsorbed nitrate has C_{2v} symmetry and is of the general form of a plane XYZ_2 molecule. The IR spectra observed in this study using pressures ranging from 8×10^{-7} to 8×10^{-4} Torr were very similar to those observed on γ-Fe_2O_3 with much higher nitric acid pressures of 3−300 mTorr.[17] Spectra were collected for blank experiments using the tungsten mesh as the background and no peaks were observed after exposure to HNO_3 as shown in Figure 13. Figure 14 shows the comparison of mass spectrometer and FT-IR data for the time dependence of the HNO_3 uptake. The two instruments are in excellent agreement, which confirms that HNO_3 lost from the gas phase is adsorbed to the surface followed by dissociation.

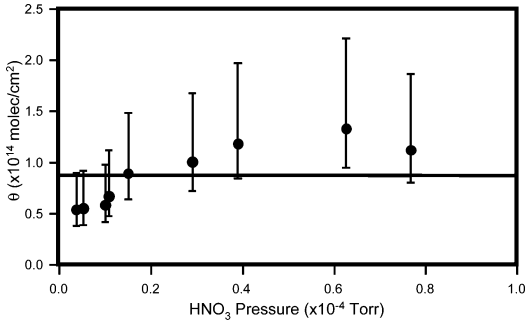

Figure 12. Saturation coverage from the pressure study at 297 K graphed as a function of standardized pressure. ($mass_{Fe_2O_3} \sim 90$ mg).

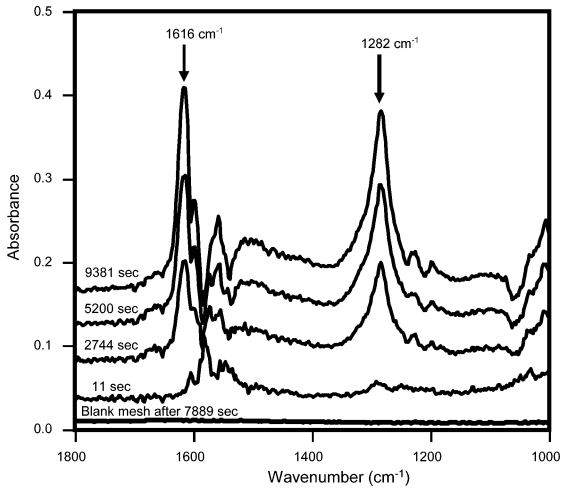

Figure 13. Growth of adsorbed nitrate peaks with time in infrared spectra during exposure of γ-Fe_2O_3 to HNO_3 ($P_{HNO_3} = 8 \times 10^{-5}$ Torr, $m_{Fe_2O_3} = 92.7$ mg, $T = 220$ K). Scales are offset for clarity. The featureless spectrum near zero is the resulting spectrum after 7889 s of exposure of a blank grid to HNO_3 ($P_{HNO_3} = 8 \times 10^{-5}$ Torr, $T = 220$ K).

IV. Conclusions and Atmospheric Implications

The specific surface area of γ-Fe_2O_3 has been measured in our vacuum chamber in situ using two independent techniques.

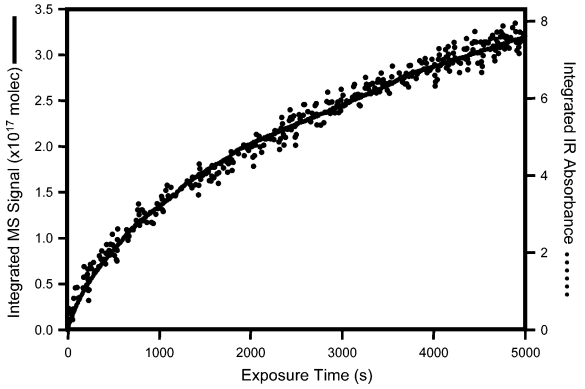

Figure 14. Comparison of MS and IR signals integrated over time. The left axis, which corresponds to the solid line, is the molecules of HNO_3 adsorbed to the surface as measured in the mass spectrometer at $m/e = 46$. The right axis, which corresponds to the dotted line, is the integrated peak area from 1100 to 1400 cm^{-1}. This peak results from adsorbed nitrate. The experimental parameters are described in the caption for Figure 13.

The measured value of 315 cm^2/mg in the linear mass regime is only slightly smaller than the manufacturer's reported BET specific surface area of 450 cm^2/mg. In the absence of in situ specific surface area measurements, the BET surface area provides a more accurate approximation than the geometric surface area.

The heterogeneous reaction between HNO_3 and γ-Fe_2O_3 has been monitored by simultaneous loss of gas-phase HNO_3 and growth of condensed phase nitrate. On the basis of the gas-phase measurements using low-mass samples, the surface coverage of adsorbed nitric acid at saturation was determined to be $(1.1 \pm 0.9) \times 10^{14}$ molecules/cm^2 at 297 K and $(1.4 \pm 0.9) \times 10^{14}$ molecules/cm^2 at 220 K. On the basis of the FT-IR data, the nitric acid was bound to the surface in the form of adsorbed nitrate. On the basis of the low mass samples, the initial uptake coefficient at $P_{HNO_3} = 1 \times 10^{-5}$ Torr was $(1.5 \pm 1.0) \times 10^{-5}$ at 297 K and $(2.9 \pm 1.0) \times 10^{-5}$ at 220 K. The coverage was enhanced only slightly at lower temperatures whereas the initial uptake coefficient was increased by almost a factor of 2.

With use of the values from this study at 297 K and with the assumption of a dust loading of 150 $\mu m^2/cm^3$,[25] a heterogeneous reaction rate coefficient (k_{het}) can be calculated using

$$k_{het} = \frac{\langle \upsilon \rangle}{4} \gamma \times SA \qquad (3)$$

where $\langle \upsilon \rangle$ is the average velocity of HNO_3, γ is the initial uptake coefficient at 297 K, and SA is the surface area of the dust event. Assuming a γ value for atmospheric dust similar to the value we find for HNO_3 on γ-Fe_2O_3 at 0% relative humidity, the lifetime of HNO_3 would be 65 days in the kinetic limit. Since dust is transported around the globe on this time scale, it is plausible that some HNO_3 is lost to the dust during transport. Of course, the uptake could be considerably faster at more atmospherically relevant relative humidities.

Assuming a concentration of HNO_3 of 100 ppt,[10] an altitude of 5 km, and the observed lack of a pressure dependence, the loss of HNO_3 from the gas phase to a mineral surface may be estimated. With use of the coverage of 8.7×10^{13} molecules/cm^2 from the pressure study, 9% of HNO_3 is expected to be removed from the gas phase. Again, this number could be even higher at higher relative humidity or on different surfaces such as clays. Studies of uptake of HNO_3 on clays at high relative humidity are ongoing.

Acknowledgment. M.A.T. would like to thank NSF-ATM 0137261 for funding; S.J.W. would like to thank Novartis and the Swiss National Science Foundation for funding; and C.J.P. gratefully acknowledges support from the CIRES Visiting Scholar Program at the University of Colorado.

References and Notes

(1) Dentener, F. J.; Carmichael, G. R.; Zhang, Y.; Lelieveld, J.; Crutzen, P. J. *J. Geophys. Res.* **1996**, *101*, 22869.
(2) Li, X.; Maring, H.; Savoie, D.; Voss, K.; Prospero, J. M. *Nature* **1996**, *380*, 416.
(3) Zhang, Y.; Carmichael, G. R. *J. Appl. Meteorol.* **1999**, *38*, 353.
(4) Prospero, J. M. *Proc. Natl. Acad. Sci. U.S.A.* **1999**, *96*, 3396.
(5) Sokolik, I. N.; Toon, O. B. *J. Geophys. Res.* **1999**, *104*, 9423.
(6) Wurzler, S.; Reisin, T. G.; Levin, Z. *J. Geophys. Res.* **2000**, *105*, 4501.
(7) Levin, Z.; Ganor, E.; Gladstein, V. *J. Appl. Meteorol.* **1996**, *35*, 1511.
(8) Hung, H.-M.; Malinowski, A.; Martin, S. T. *J. Phys. Chem. A* **2003**, *107*, 1296.
(9) Seinfeld, J. H.; Pandis, S. N. *Atmospheric Chemistry and Physics from Air Pollution to Climate Change*; John Wiley: New York, 1998.
(10) Tabazadeh, A.; Jacobson, M. Z.; Singh, H. B.; Toon, O. B.; Lin, J. S.; Chatfield, R. B.; Thakur, A. N.; Talbot, R. W.; Dibb, J. E. *Geophys. Res. Lett.* **1998**, *25*, 4185.
(11) Underwood, G. M.; Miller, T. M.; Grassian, V. H. *J. Phys. Chem. A* **1999**, *103*, 6184.
(12) Ennas, G.; Marongiu, G.; Musinu, A.; Falqui, A.; Ballirano, P.; Caminiti, R. *J. Mater. Res.* **1999**, *14*, 1570.
(13) Fine, P.; Singer, M. J.; Verosub, K. L.; TenPas, J. *Soil Sci. Soc. Am. J.* **1993**, *57*, 1537.
(14) Liu, X. M.; Hesse, P.; Rolph, T. *Phys. Earth Planet. Inter.* **1999**, *112*, 191.
(15) Ketterings, Q. M.; Bigham, J. M.; Laperche, V. *Soil Sci. Soc. Am. J.* **2000**, *64*, 1108.
(16) Underwood, G. M.; Li, P.; Al-Abadleh, H.; Grassian, V. H. *J. Phys. Chem. A* **2001**, *105*, 6609.
(17) Goodman, A. L.; Bernard, E. T.; Grassian, V. H. *J. Phys. Chem. A* **2001**, *105*, 6443.
(18) Hanisch, F.; Crowley, J. N. *J. Phys. Chem. A* **2001**, *105*, 3096.
(19) Hanisch, F.; Crowley, J. N. *Phys. Chem. Chem. Phys.* **2001**, *3*, 2474.
(20) Underwood, G. M.; Song, C. H.; Phadnis, M.; Carmichael, G. R.; Grassian, V. H. *J. Geophys. Res.* **2001**, *106*, 18055.
(21) Newman, A. C. D. *J. Soil Sci.* **1983**, *34*, 23.
(22) Downing, H. D.; Williams, D. *J. Geophys. Res.* **1975**, *80*, 1656.
(23) Al-Abadleh, H. A.; Grassian, V. H. *J. Phys. Chem. A* **2000**, *104*, 11926.
(24) Herzberg, G. *Molecular Spectra and Molecular Structure II. Infrared and Raman Spectra of Polyatomic Molecules*, 13th ed.; D. Van Nostrand: New York, 1968.
(25) de Reus, M.; Dentener, F.; Thomas, A.; Borrmann, S.; Ström, J.; Lelieveld, J. *J. Geophys. Res.* **2000**, *105*, 15263.